Finite Element Analysis of Ultrasonic Processing of a Polymer-Matrix Composite

Wenguang Zhao[1], David Roylance[2], John Player[3]

Abstract

Viscoelastic heating induced by ultrasonic loading is an attractive method of consolidating polymer-matrix composites. An ultrasonically oscillating loading horn is applied to a small region at the laminate surface, which produces a spatially nonuniform strain energy field within the material. A fraction of this strain energy is dissipated during each ultrasonic loading cycle depending on the temperature-dependent viscoelastic response of the material. This dissipation produces a rapid heating, yielding temperature increases near 100^{o}C in approximately 1s and permitting the laminate to be consolidated prior to full curing in an autoclave or other equipment. The spatially nonuniform, nonlinear, and coupled nature of this process, along with the large number of experimental parameters, makes trial-and-error analysis of the process difficult, and this paper demonstrates how a finite-element simulation can be valuable in process development and optimization.

Keywords: Fiber-reinforced composites; Ultrasonic Tape Lamination; Viscoelastic dissipation; Finite-element analysis

---

1. Introduction

This paper explores a ultrasonic heating technique in which a probe tip oscillating at ultrasonic frequency of 20-40 KHz is applied to the surface of the uncured part to cause a cyclic indentation. A fraction of the induced strain energy is dissipated as heat due to the material's viscoelastic properties. This also generates the pressure needed for the consolidation stage in the cure cycle. The ultrasonic consolidation relieves some of the necessity for autoclave consolidation and cure, which is an expensive and inflexible technology.

[1] Dept. of Civil and Environmental Engineering, Massachusetts Institute of Technology, Cambridge, MA 02139.
[2] Dept. of Materials Science and Engineering, Massachusetts Institute of Technology, Cambridge, MA 02139.
[3] InfoSciTex Corp., Waltham, MA 02154.

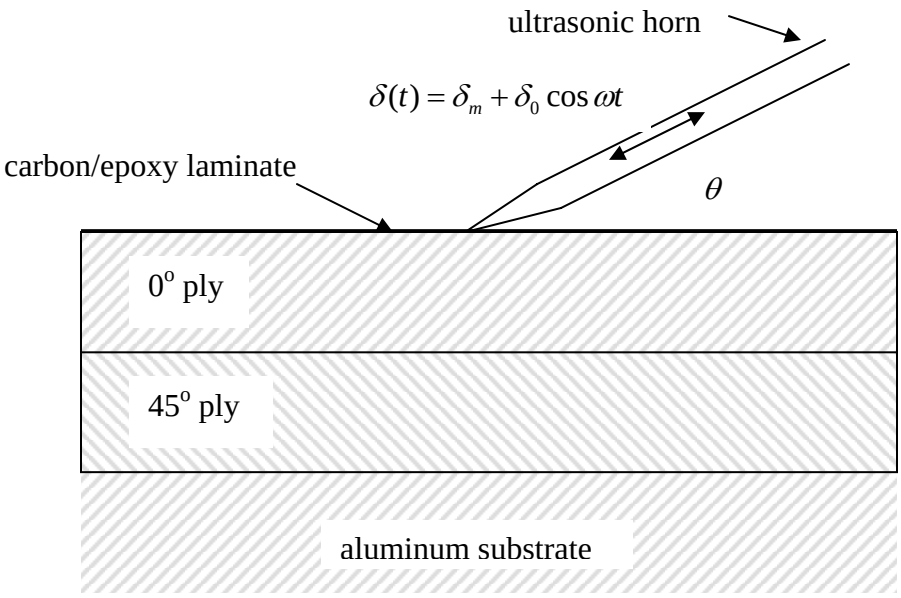

Fig. 1 - Schematic of fixture for ultrasonic heating studies.

Figure 1 shows a schematic of the loading fixture used in static experimental ultrasonic heating studies, in which the horn is not moved along the surface of the laminate during processing. (The FEA model has the capability of simulating a moving horn that moves laterally during processing, but this aspect of the study in not included here.) The laminate studied in this paper is a simple one with only two plies, the top ply having fibers oriented in the 0^o direction and the lower having a fiber orientation 45^o from the top.

The heating rate induced by the ultrasonic loading horn is a strong function of several experimental variables, notably the amplitude δ_0 of the oscillatory displacement, the frequency ω and the horn angle θ [1, 2]. The superimposed mean displacement δ_m has only a minor influence on the heating rate, but is important in consolidation of the laminate as the material is softened by the heating. Excessive oscillatory or mean loads can damage the laminate, which of course must be avoided. Experiments have shown that the amplitude of the oscillatory displacement should be in the range 15 - 60 μm, and the mean load should be 5 – 50 N. A substantial shearing component of the applied load is beneficial for effective heating, and horn angles in the range 20^o – 40^o from the horizontal are typical.

The ultrasonic heating process is complex, having many experimental parameters such as ultrasonic horn angle, frequency, oscillation amplitude, density, specific heat, and others. This makes process optimization by experimentation alone expensive and time-consuming. Theoretical modeling such as finite element analysis (FEA) is very useful this case, and helps elucidate the interplay of the coupled and nonlinear physical phenomena involved.

2. Prior modeling studies

A web module by Roylance [3] outlines the Galerkin approach to finite element analysis to simulations of various polymer and composite processing operations, to include non-isothermal, reactive, and transient viscous flow processes. Other useful work in modeling nonisothermal processing operations includes the following:

Pusatcioglu et al. investigated the temperature gradient developed during the casting of unsaturated polyester by solving the one-dimensional heat transfer equation using experimentally determined reaction kinetics and thermal conductivities [4]. Lee and Springer presented a one-dimensional analytical cure model for prepreg composites. A finite-difference cure-modeling program based on this model uses implicit method to calculate the degree of cure and, it can also analyze the tool and the bagging [5]. Bogetti and Gillespie studied two-dimensional anisotropic cure simulations of thick thermosetting composites using boundary fitted co-ordinate systems with the finite-difference technique [6]. The solution was reported to be mesh-dependent. Young investigated the resin-transfer molding process and developed a six-node wedge element to model the non-isothermal mould filling [7]. Loos and Springer developed a one-dimensional finite difference model to simulate the cure process of a flat plate [8]. Based on their finite difference modeling, Loos and MacRae followed to develop a two-dimensional finite element model to simulate the resin film infusion process including curing [9]. Yi et al. developed a nonlinear transient heat transfer FE model to simulate the curing process of polymer matrix composites. Temperature field inside the laminates was evaluated by solving the nonlinear anisotropic heat conduction equations including internal heat generation produced by exothermic chemical reactions [10]. Joshi et al. used a general-purpose FE package for cure modeling. Application of transient heat-transfer analysis is demonstrated by modeling the cure of thick prepreg laminate, a honeycomb sandwich panel and an I-beam. Stability with respect to the FE density and the length of the time step employed is also investigated [11].

3. Material Characterization

The study material in this project was CYCOM 977-3, a popular high-performance carbon-epoxy composite intended for military and other demanding aerospace applications. At the vendor's request, we did not use analytical methods to "deformulate" this material; however, it is commonly stated in the composites community that 977-3 is probably a thermoplastic-toughened TGMDA/DDS (tetraglycidyl methylene dianiline/diamino-diphenyl sulfone) epoxy. These epoxy constituents are shown in Fig. 2 below.

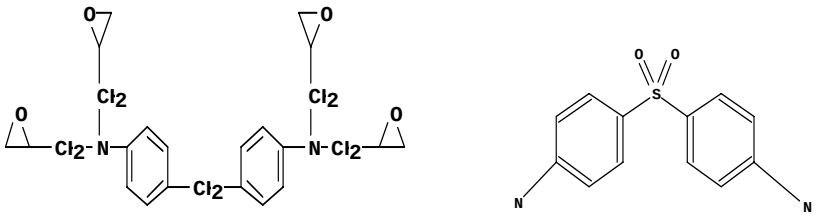

Fig. 2 - Chemical structure of TGMDA (left) and DDS.

This chemical structure is consistent with the FTIR (Fourier transform infrared spectroscopy) results shown in Fig. 3 below. FTIR was also used to study the salient features of the resin curing reaction. (This paper reports only on the viscoelastic heating used in laminate consolidation, but the FEA code to be described here is also able to simulate the curing process; the FTIR observations are useful in determining the parameters needed in these curing studies.)

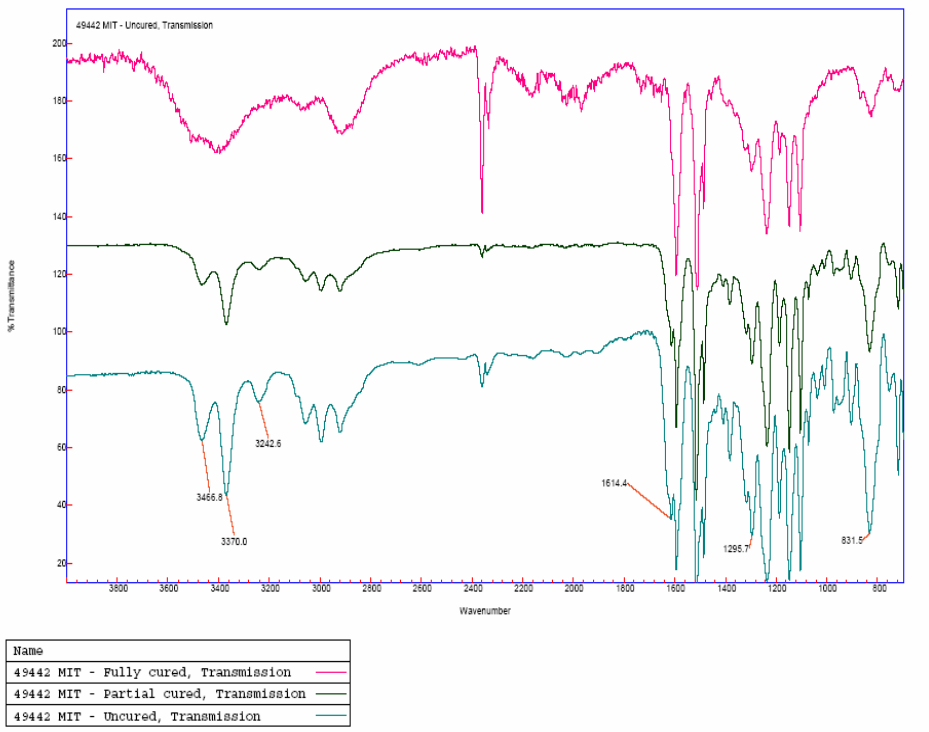

Figure 3. FTIR spectra for the study epoxy resin.

The functional groups indicate by these spectra are consistent with a TGMDA/DDS resin: 831.5 wave number, epoxy ring -C-C-O-; 1614.4, -NH2; three peaks from 3242 to 3466, -NH2; a broad peak at ~3400, -OH with hydrogen bonding; three peaks at ~3000, -CH-, -CH2-; 1295.7, SO2. As expected, the peak of the epoxy ring -C-C-O- decreases with the curing process while the concentration of -OH increases.

Because the manufacturer-supplied curing temperature of CYCOM 977-3 is 177°C (350°C) and the temperature fields in the ultrasonic heating simulations are below 150°C, the cure reaction is not included in the model results presented below. The FEA results reported here considered only the consolidation stage of the laminates due to the viscoelastic dissipation, without considering the internal heat generation produced by exothermic chemical reactions. This conclusion is consistent with calorimetric studies conducted in the present work and also in Ref. 1.

Resin viscoelastic response was characterized by Dynamic Mechanical Analysis (DMA). Eight plies were stacked and measured in the oscillatory compression mode. The frequency was fixed at 1 Hz and the temperature was swept from 25°C to 230°C. The result is shown in Fig. 4. The peak of the loss modulus indicates a glass transition temperature (T_g) at approximately 75°C for the uncured resin, which results in the viscoelastic heating induced by ultrasonic loading increasing as the specimen temperature rises to T_g, and diminishing thereafter.

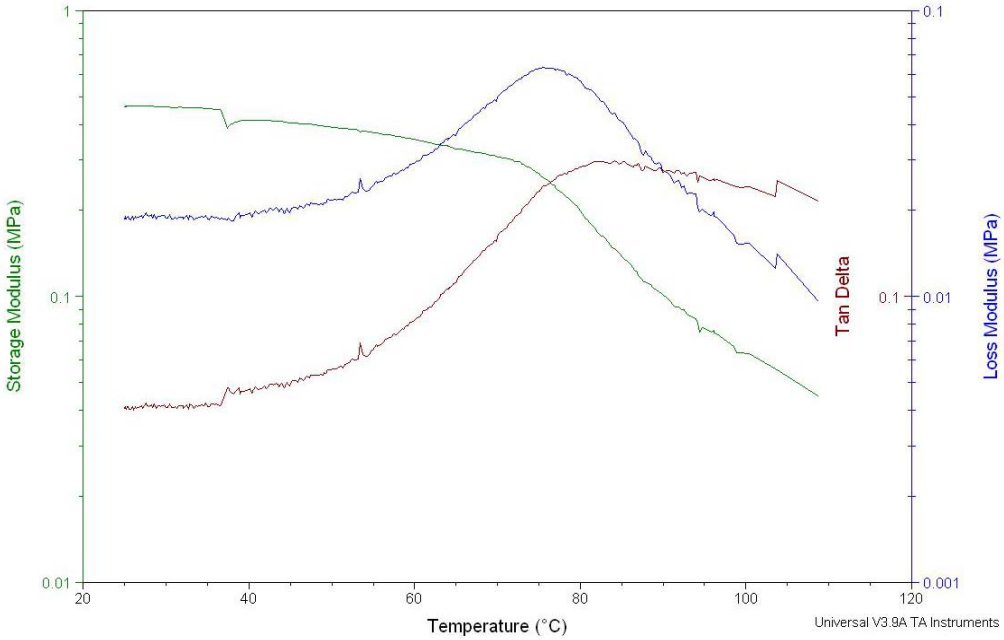

Fig. 4 - DMA spectra for uncured 977-3 carbon/epoxy composite.

DMA spectra can be used to develop an analytical expression for the temperature and frequency dependence of the viscoelastic response, and the finite element formulation to be described below was written to incorporate a Wiechert-type discrete form of the dynamic behavior [12]:

$$E' = k_0 + \sum_{j=1}^{N} \frac{k_j (\omega \tau_j)^2}{1 + (\omega \tau_j)^2}$$

$$E'' = \sum_{j=1}^{N} \frac{k_j(\omega\tau_j)}{1+(\omega\tau_j)^2}$$

Here ω is the frequency of cyclic loading and the k_j and τ_j are spring stiffnesses and relaxation times for each element in the model. Idealizing the material as "thermorheologically simple," the temperature dependence can be written by taking the relaxation times to obey an Arrhenius relation of the form:

$$\tau_j = \tau_{0j} \exp\left(\frac{E^\tau}{R_g T}\right)$$

where T is the temperature, τ_{0j} are preexponential constants, E^τ is an apparent activation energy that is the same for each element, and $R_g = 8.314$ J/mol is the gas constant. Numerical values for τ_{0j}, k_j and E^τ were fit to the DMA data in Ref. 1 for a similar resin as:

τ_{0j} (s)	k_j (Pa)
8.87E-11	1.11E+06
8.87E-12	5.56E+06
8.87E-13	1.03E+07
8.87E-14	2.50E+07
8.87E-15	8.42E+07
8.87E-16	2.10E+08
8.87E-17	2.87E+07

The activation energy was determined by the line slope of an Arrhenius plot of $\log\tau_j$ vs. $1/T$ for the DMA data to be E^τ = 69.1 kJ/mol.

3. Numerical Model

3.1 *Governing equations for temperature*

The time- and spatially-dependent heat generation rate in ultrasonic loading is governed by the well-known conservation equation for energy [13]

$$\rho c \frac{\partial T}{\partial t} = Q + \nabla\left(\mathbf{k}\nabla T\right)$$

where ρ is density (kg/m^3), c is specific heat (J/kg-K), Q is heat generation rate (W/m^3), $\mathbf{k} = \left(k_x, k_y\right)$ is the anisotropic thermal conductivity (W/m-K), and $\nabla^{\mathrm{T}} = \left(\partial/\partial x, \partial/\partial y\right)$ is the gradient operator. We model the composite as a homogeneous system with both fiber and matrix having the same temperature during the heating

process. As resin chemical reaction is negligible for the times and temperatures of the simulations discussed here, the heat generation Q arises only from the viscoelastic dissipation as [14]:

$$Q = f \cdot W_{dis} = f \cdot \frac{E''}{E'} \cdot W_{st}$$

where f is the frequency (Hz), W_{dis} is the net dissipation per cycle, and W_{st} is the maximum stored energy per cycle (both J/m^3). E' is the storage modulus and E'' is the loss modulus (both Pa).

3.2 *Governing equations for displacement*

The actual ultrasonic loading event is three dimensional, with the horn appearing somewhat as a wide screwdriver blade; the ends of the blade obviously produce a different loading than the central region. To simplify the analysis, the FEA model simulates the central region, where the loading can be idealized as one of plane strain.

Our numerical model does not follow the loading continuously during the ultrasonic cycle, but simply computes the magnitude of energy dissipated per cycle. The spatially-dependent strain energy density W_{st} is computed using a conventional FEA displacement approach, based on a point displacement at the surface of amplitude equal to the maximum amplitude of the cyclic ultrasonic displacement. The superimposed mean loading is not considered.

The stresses $\boldsymbol{\sigma}$, strains $\boldsymbol{\varepsilon}$ and displacements $\mathbf{u}$ are given in matrix-vector notation for Hookean materials in small strain as [15, 16]:

$$\boldsymbol{\sigma} = \begin{Bmatrix} \sigma_x \\ \sigma_x \\ \tau_{xy} \end{Bmatrix}, \quad \boldsymbol{\varepsilon} = \begin{Bmatrix} \varepsilon_x \\ \varepsilon_x \\ \gamma_{xy} \end{Bmatrix}, \quad \mathbf{u} = \begin{Bmatrix} u_x \\ u_y \end{Bmatrix},$$

$$\mathbf{L}^{\mathrm{T}}\boldsymbol{\sigma} = \mathbf{L}^{\mathrm{T}}\mathbf{D}\boldsymbol{\varepsilon} = \mathbf{L}^{\mathrm{T}}\mathbf{D}\mathbf{L}\mathbf{u} = \mathbf{0}$$

where $\mathbf{L}$ is a matrix of differential operators, given for 2-D Cartesian problems as:

$$\mathbf{L} = \begin{bmatrix} \partial/\partial x & 0 \\ 0 & \partial/\partial y \\ \partial/\partial y & \partial/\partial x \end{bmatrix}$$

and $\mathbf{D}$ is a stiffness matrix of material constants. For transversely isotropic materials in plane strain, $\mathbf{D}$ takes the form

$$\mathbf{D} = \frac{E_2}{(1+\nu_1)(1-\nu_1-2n\nu_2^2)} \begin{bmatrix} n(1-\nu_2^2) & n\nu_2(1+\nu_1) & 0 \\ n\nu_2(1+\nu_1)(1-\nu_1^2) & (1-\nu_2^2) & 0 \\ 0 & 0 & m(1+\nu_1)(1-\nu_1-2n\nu_2^2) \end{bmatrix}$$

where E_1, G_1, ν_1 are tensile and shear moduli and Poisson's ratio in the plane of the laminate and E_2, G_2, ν_2 the corresponding parameters in the laminate through-thickness direction. We also have

$$\frac{E_1}{E_2} = n, \text{ and } \quad \frac{G_2}{E_2} = m$$

This form of **D** applies when the fiber direction is aligned with the *x*-axis. For other ply orientations, the stiffness matrix must be transformed using standard methods [16] from the fiber direction to the common *x-y* axes used for the overall laminate.

3.3 *Finite element formulation*

The governing equations for temperature and displacement can be transformed to their finite element counterparts using the Galerkin procedure described in FEA texts [15]. Briefly, the unknown temperature and displacement functions are approximated by a polynomial interpolation of "nodal" values (T_i, $\mathbf{u}_i$) at selected points within discrete finite elements:

$$T(x, y) \approx \Sigma N_i T_i$$
$$\mathbf{u}(x, y) \approx \Sigma N_i \mathbf{u}_i$$

where N_i are interpolation functions (linear in our analysis). These approximations are substituted into the closed-form governing equations, and the residual error minimized by integrating the resulting expressions over the element volume. This produces a set of nonlinear equations for the nodal unknowns of the form

$$\mathbf{Ka} = \mathbf{f}$$

where **a** is a vector of the nodal temperatures and displacements, **f** is vector of nodal heat fluxes and forces, and **K** is a "stiffness" matrix relating these two quantities. The thermal and mechanical components of the stiffness matrix are:

$$\mathbf{K}_{\mathrm{T}} = \int_{\Omega} \left(\nabla^T \mathbf{N}\right) \rho c \nabla \mathbf{N} \, d\Omega, \qquad \mathbf{K}_u = \int_{\Omega} \mathbf{B}^{\mathbf{T}} \mathbf{D} \mathbf{B} \, d\Omega$$

where $\mathbf{B} = \mathbf{L}\mathbf{N}$. The right-hand side vector **f** is formed as

$$\mathbf{f}_T = -\int_\Omega \mathbf{N} Q \, d\Omega, \;\; \mathbf{f}_u = -\int_\Omega \mathbf{B}^{\mathrm{T}} \boldsymbol{\sigma} \, d\Omega$$

The integrals in the above relations are evaluated by Gauss-Legendre numerical methods [15], which entail evaluating the integrands at optimally located "Gauss points" within each element volume Ω.

3.4 Transient analysis

To model the time dependence of the process, the FEA model is extended as

$$\mathbf{C}\dot{\mathbf{a}} + \mathbf{K}\mathbf{a} = \mathbf{f}$$

where the overdot indicates the time derivative and the "inertia" matrix **C** is

$$\mathbf{C}_{\mathrm{T}} = \int_\Omega \mathbf{N}^T \rho c \, \mathbf{N} \, d\Omega$$

A two-point recursion approach [15] can be used to solve the transient equations:

$$\mathbf{C}\frac{\mathbf{a}_{n+1} - \mathbf{a}_n}{\Delta t} + \mathbf{K}\left[\left(1-\theta\right)\mathbf{a}_n + \theta \mathbf{a}_{n+1}\right] = \mathbf{f}$$

where the subscripts n and $n+1$ indicate values of the nodal solution vector before and after a discrete time increment Δt. This expression gives a conventional forward difference scheme for $\theta = 1$, backward differencing for $\theta = 0$, and a Galerkin scheme for $\theta = 2/3$. The Galerkin scheme is unconditionally stable, and was used in all our analyses.

The FEA model is able to adjust the time increment arbitrarily as the analysis proceeds. We have found this to be very important in these ultrasonic heating simulations, as too large an increment produces a thermal overshoot that then destroys the accuracy of subsequent time steps. We have found it useful to use logarithmic stepping, with very small increments, at the beginning of the simulations. As the temperature field becomes established, the logarithmic stepping gives larger and more economic increments. Toward the end of the analysis, the time steps can become constant. The choice of workable time-stepping parameters is dependent on material and geometrical parameters as well as mesh size, and this is perhaps the most difficult aspect of FEA modeling of ultrasonic heating.

4. Numerical simulations

4.1 Laminate geometry and material properties

As illustrated in Fig. 1, the experimental laminate modeled in the simulations reported here consisted of two layers each 360 μm thick, both of CYCOM 977-3 carbon-epoxy prepreg. The orientation of the upper layer was 0^o (fibers oriented axially along the

substrate) and the lower was 45°. The frequency of the ultrasonic horn was 30 KHz with amplitude 16 μm, and a static contact load of 1.44 N. The horn angle θ was 30°.

Using handbook and vendor data, the material density was taken as 2000 kg/m^3 and the specific heat as 116 J/kg-K. The thermal conductivity k_x in the fiber direction is 18.0 W/m-K and k_y in the through-thickness direction is 0.95 W/m-K; these values were used directly for the 0° top layer of the two-ply laminate. In the lower 45° ply k_y remains the same but the appropriate axis transformation gives k_x = 0.95 W/m-K.

Also using vendor data, the top 0° ply has an elastic modulus of 162 GPa, a shear modulus of 4.96 GPa, and Poisson's ratio of 0.27; for the second layer the elastic modulus is 16.94 GPa, the shear modulus is 41.6 GPa, and the Poisson's ratio is 0.806.

4.1 Finite Element Model

The rectangular-element mesh shown in Fig 5 was used in all of our simulations; this element shape facilitated studies not reported here in which the horn is moved laterally along the laminate surface as the process continues. The mesh is graded to provide increased resolution at the loading point (center top of the mesh). Displacements were fixed at zero along the bottom and sides of the mesh, and the temperature was fixed at 23°C along the bottom to simulate the large thermal inertia of the aluminum substrate. All nodes were set to an initial temperature of 23°C. The FEA code is able to simulate convective heat transfer from the upper free surface, but this effect was not included in the simulations reported here.

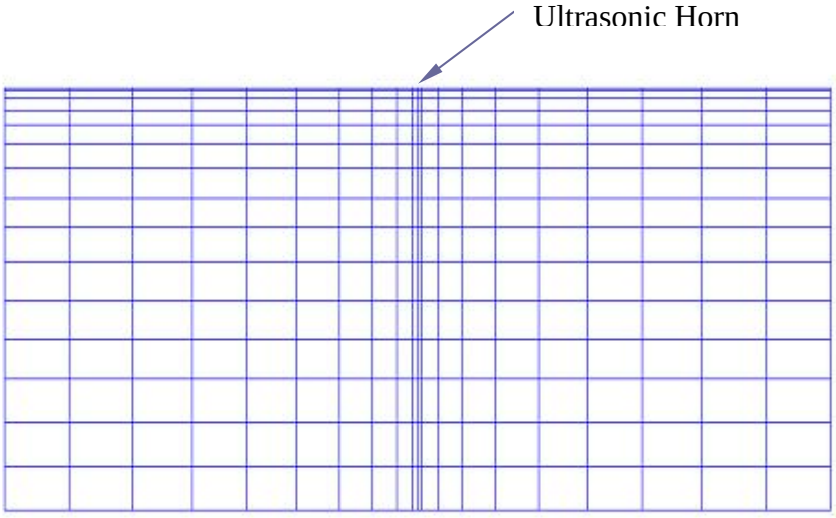

Fig. 5 - Two-dimensional finite element model in gradient mesh

The FEA model is sufficiently complex that verification of its accuracy and reliability is difficult. One important test of the model is aimed at obtaining a reasonable agreement

of the predicted displacement field with the theoretical analysis of Flamant [17], who developed a plane-strain analysis for a vertical point load on a semi-infinite half plane. The numerical prediction of the FEA model is compared with the Flamant solution in Figs. 6. Agreement is fair, with more error in the high-gradient region near the loading point.

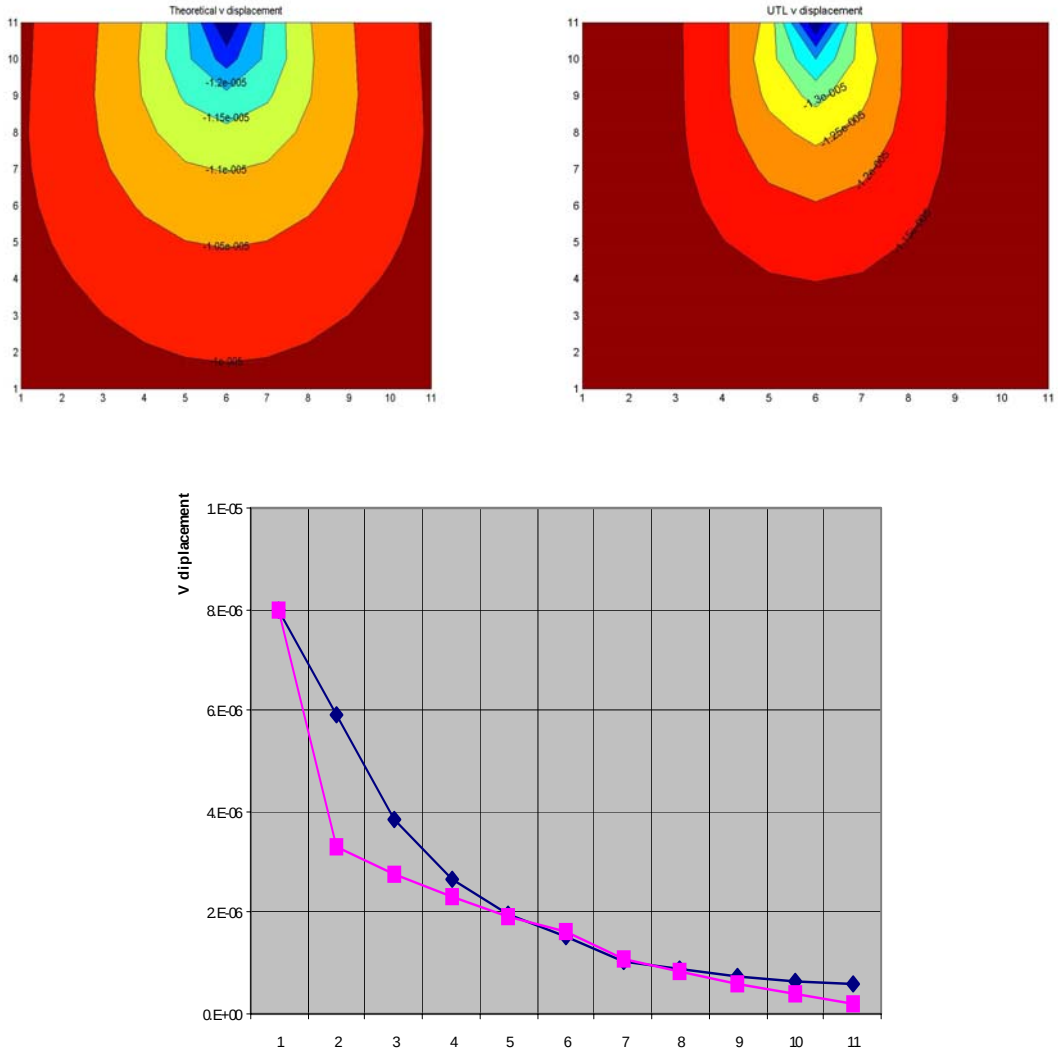

Fig. 6 - Plots of vertical deflection vs. depth beneath the loading point for the theoretical Flamant plane-strain analysis (black, diamonds) and FEA numerical model (red, rectangles).

Other checks against classical closed-form solutions were also carried out, such as a comparison with the one-dimensional transient heat conduction equation. These were useful in locating and removing errors in theory and coding. For more complex situations in which no closed-form analysis is available, simple geometries were used to check the "reasonableness" of the numerical results. As an example, Fig. 7 displays a

FEA temperature field for a single layer of material at an early time in the heating program. The field is nonsymmetric due to the inclined loading horn.

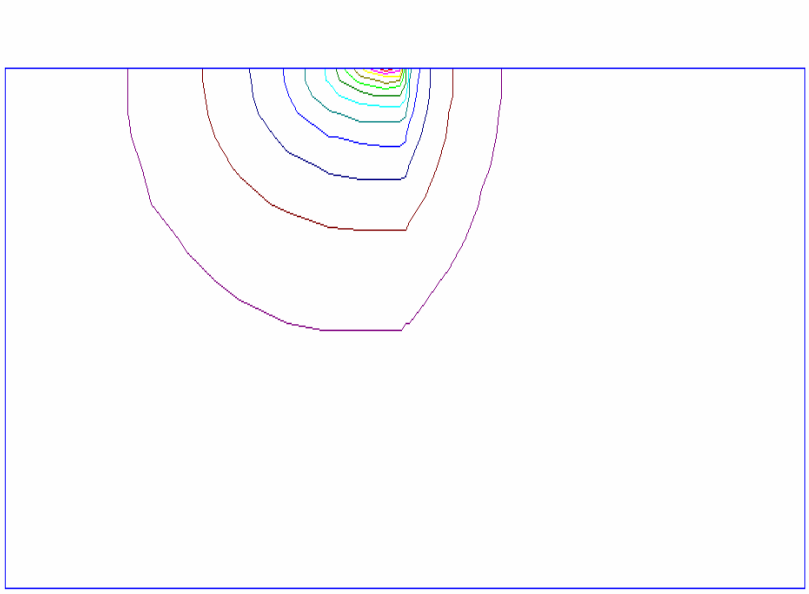

Fig. 7 - Temperature contours at t = 0.6s in a single material layer. ; The contours represent equal increments of temperature from a maximum of 26^{o}C (red, closest to loading point) to 23^{o}C (violet).

Fig. 8 shows an experimental setup to obtain data for model verification and fine-tuning. Here the horn is not moved laterally along the laminate as would be done in actual ultrasonic consolidation, and the surface temperature was monitored by two thermo-couples and an infrared sensor. The frequency of the ultrasonic horn here was 30 kHz, the horn angle was 30°, the oscillatory amplitude was 16 μm and the superimposed contact load was 28.5 N.

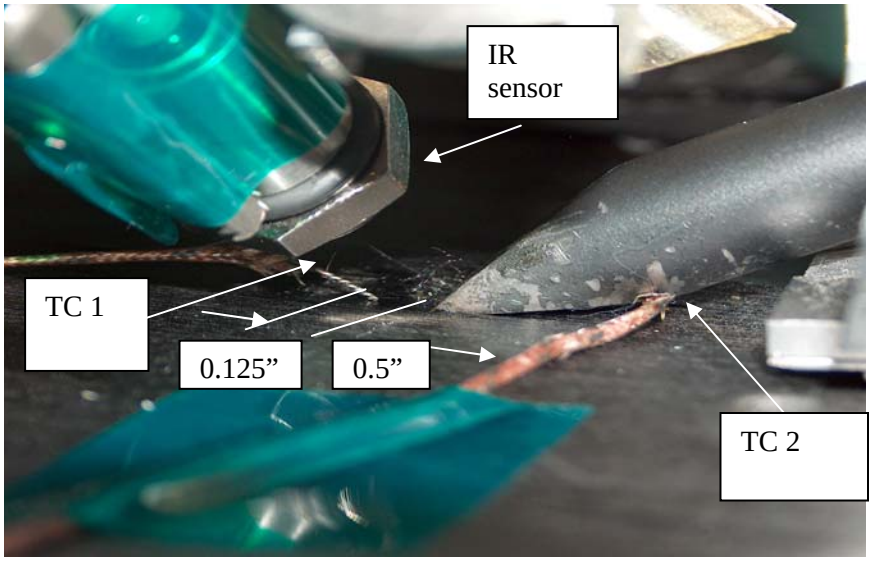

Fig. 8 - Experimental setup to monitor surface temperature during ultrasonic heating.

Fig. 9 shows the comparison between the FEA temperature histories at the loading point with the experimental infrared and thermocouple readings. The experimental values plateau eventually at approximately 60^{o}C, probably because the viscoelastic dissipation diminishes as the material heats above its T_g and also because the surface temperature is increasingly effected by heat loss from the surface by convection. This FEA simulation does not include surface convection, so the numerical temperature predictions tend to increase to unrealistic values with time. It is clear that the numerical and experimental values are of the same magnitude, but also show substantial disagreement in both numerical values and their time histories. Further development of both the experimental sensor instrumentation and the FEA model is required for better agreement.

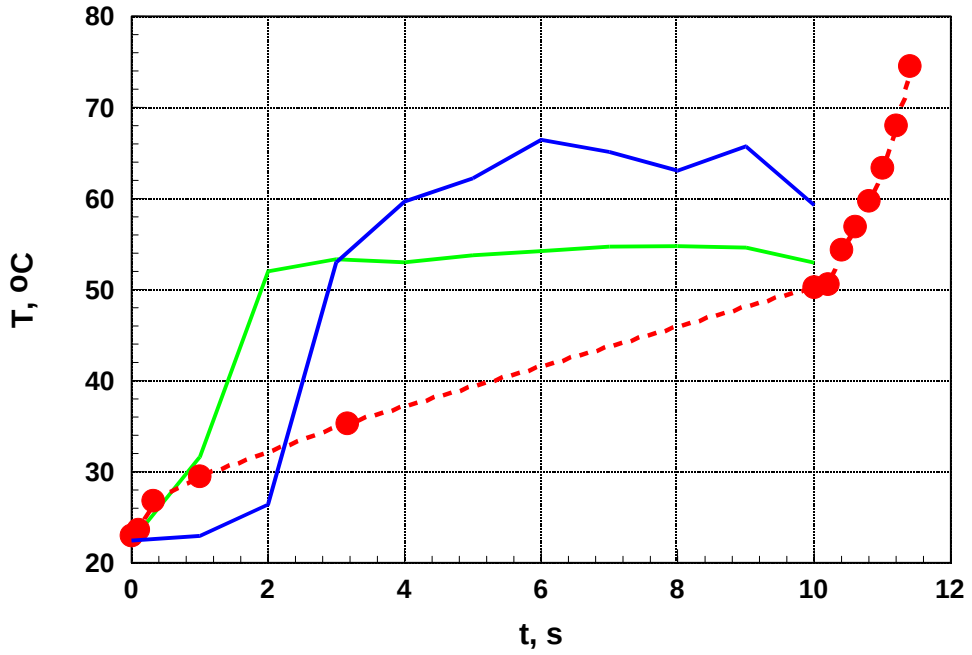

Fig. 9 – Comparison of experimental and FEA temperature histories below loading point; green – IR sensor; blue – thermocouple; red – FEA.

5. Conclusions

Ultrasonic heating has a number of advantages compared with conventional autoclave procedures for laminate consolidation and repair. However, the very large number of experimental parameters - horn angle, oscillation amplitude, velocity of horn along the surface, thickness and material properties of the laminate, etc. – make a purely trial-and-error approach to process development and optimization difficult. FEA simulation is helpful in intuiting the effect of experimental parameters on system response, though further experience with such model parameters as mesh size, time step and boundary conditions would render the FEA model more reliable and easier to apply to changing experimental conditions.

Acknowledgments

This work was supported by a teaching and research collaboration between the Massachusetts Institute of Technology and the Malaysian University of Science and Technology. It is the subject of the MIT SM thesis of W. Zhao (18), who was supported by the MIT-MUST program as well. The authors also acknowledge the kind assistance of Cytec Corp. in supplying the 977-3 study material.

References

1. Roylance, M., J. Player, W. Zukas, and D. Roylance, "Modeling of Ultrasonic Processing," *Journal of Applied Polymer Science*, Vol. 93, pp. 1609-1615, 2004.
2. M. N. Tolunay, P. R. Dawson and K. K. Wang, "Heating and Bonding Mechanism in Ultrasonic Welding of Thermoplastics," *Polymer Engineering and Science*, Vol. 23, No. 13, pp. 726-733, 1981.
3. D. Roylance, *Finite Element Analysis of Nonisothermal Reactive Flows*, http://web.mit.edu/course/3/3.064/www/slides/flow.pdf, 2003.
4. S. Y. Pusatcioglu, J. C. Hassler, A. L. Frickle and H. A. MeGee Jr., "Effect of Temperature Gradients on Cure and Stress Gradients in Thick Thermoset Castings, *Journal Applied Polymer Science*, Vol. 25, pp. 381-393. (1980).
5. W. I. Lee, A. C. Loos and G. S. Springer, "Heat of Region, Degree of Cure, and Viscosity of Hercules 3501-6 Resin," *Journal of Composite Materials*, Vol. 16, pp. 10-520, 1982.
6. T. A. Bogetti and J. W. Gillespie Jr., "Two-Dimensional Cure Simulation of Thick Thermosetting Composites," *Journal of Composite Materials*, Vol. 25, 239-273, 1991.
7. W. B. Young, "Thermal Behavior of the Resin and Mold in the Process of Resin Transfer Molding," *Journal of Reinforced Plastic Composites*, Vol. 14, pp. 310-332, 1995.
8. A. C. Loos and G. S. Springer, "Curing of Epoxy Matrix Composites" *Journal of Composite Materials*, Vol. 17, pp. 135-169, 1983.
9. A. C. Loos and J. D. MacRae," A Process Simulation Model for the Manufacturing of a Blade-Stiffened Panel by the Resin Film Infusion Process," *Composite Science and Technology*, Vol. 56, 273-289, 1996.
10. S. Yi *et al*. "A Finite Element Approach for Cure Simulation of Thermosetting Matrix Composites," *Computers and Structures*, Vol. 64. No. 1-4. pp. 383-388, 1997.
11. S. C. Joshi *et al*. "A Numerical Approach to the Modeling of Polymer Curing in Fiber-Reinforced Composites," *Composite Science and Technology*, Vol. 59, pp. 1003-1013, 1999.
12. D. Roylance, *Engineering Viscoelasticity*, http://web.mit.edu/course/3/3.11/www/modules/visco.pdf, 2001.
13. R.B. Bird, W.E. Stewart, and E.N. Lightfoot, *Transport Phenomena*, J. Wiley & Sons, New York, 1960.
14. N.G. McCrum, B.E. Read and G. Williams, Anelastic and Dielectric Effects in Polymeric Solids, J. Wiley & Sons, New York, 1967.
15. O. C. Zienkiewicz, "The Finite Element Method," McGraw-Hill, 1997.
16. D. Roylance, *Mechanics of Materials*, J. Wiley & Sons, New York, 1996.
17. S. Timoshenko and J. Goodier, *Theory of Elasticity*, McGraw-Hill, New York, 1951.
18. W. Zhao, *Modeling of Ultrasonic Processing*, S.M. Thesis, MIT, Cambridge, MA, August 2005.